

Refracting Metasurfaces without Spurious Diffraction

Guillaume Lavigne, Karim Achouri, Viktor Asadchy, Sergei Tretyakov, and Christophe Caloz

Abstract—Refraction represents one of the most fundamental operations that may be performed by a metasurface. However, simple phase-gradient metasurface designs suffer from restricted angular deflection due to spurious diffraction orders. It has been recently shown, using a circuit-based approach, that refraction without spurious diffraction, or diffraction-free, can fortunately be achieved by a transverse (or in-plane polarizable) metasurface exhibiting either loss-gain, nonreciprocity or bianisotropy. Here, we rederive these conditions using a medium-based – and hence more insightful – approach based on Generalized Sheet Transition Conditions (GSTCs) and surface susceptibility tensors, and experimentally demonstrate two diffraction-free refractive metasurfaces that are essentially lossless, passive, bianisotropic and reciprocal.

I. INTRODUCTION

Metasurfaces represent a powerful electromagnetic technology that has experienced spectacular development over the past lustrum [1], [2], [3]. They have already lead to a diversity of applications, including single-layer perfect absorption [4], polarization twisting [5], power harvesting [6], orbital angular momentum multiplexing [7], [8], spatial processing [9] and flat lensing [10], and there seems to be much more to be discovered and developed in this area.

One of the most fundamental operations that a metasurface may perform is generalized refraction and reflection [11], as most metasurface field transformations involve these phenomena. Such operations have been achieved in *blazed gratings* [12], [13], and later in *planar phase-gradient metasurfaces* [11], however with restriction to small angle differences between the incident and refracted or reflected beams and with the presence of spurious diffraction orders [8], [14], [15], [16].

Fortunately, it is possible to achieve refraction without spurious diffraction, that we shall hereafter refer to as *diffraction-free* refraction for short, by introducing more complexity in the metasurface design. This has been clearly demonstrated in [14], which shows that such operation may be accomplished by a *transverse*¹ metasurface if that metasurface exhibits any one of the following three properties:

- 1) monoisotropy with loss and gain [18],
- 2) nonreciprocity [14], or
- 3) bianisotropy [19], [20], [21].

Among these properties, the practically most convenient is certainly the third one, since it allows to achieve diffraction-free generalized refraction with a metasurface that is purely lossless and passive, avoiding complex amplification, and at the same time reciprocal, avoiding non-integrable magnetic materials [22] or complex magnetless structures [23], [24], [25].

The work reported in [19], and related experimentation [20], represents the first synthesis of a diffraction-free generalized refractive metasurface. In that paper, the authors use a *circuit-based* approach with generalized scattering parameters to match the impedances of the

¹A transverse metasurface is a metasurface characterized only by tensor components that are parallel to the plane of the metasurface (i.e. “in-plane” or \parallel) or, equivalently, perpendicular to the normal of the metasurface. Including longitudinal (i.e. “off-plane” or \perp) tensor components, i.e. components in the direction of the normal of the metasurface, immediately brings about much greater complexity because, as shown in [17], this transforms otherwise algebraic GSTC equations into differential equations. The reduction of the general to a transverse metasurfaces reduces the four bianisotropic constitutive parameters from 3×3 tensors ($4 \times 9 = 36$ elements) to 2×2 tensors ($4 \times 4 = 16$ elements).

oblique incident and transmitted waves across a *layered* metasurface structure. As a result, they obtain analytical expressions for the admittances of each of the layers constituting the metasurface. Here, as an extension of the short report [21], we present a fundamentally different and also more general approach of the same problem. This approach uses surface susceptibilities synthesized [26], [17], [27] by Generalized Sheet Transition Conditions (GSTCs) [28], and is therefore a *medium-based* rather than a circuit-based approach, which inherently brings about greater insight into the physics of the problem. Moreover, it treats the metasurface as a *global entity*, without any restriction regarding its structure, and may therefore accommodate different implementations, via subsequent scattering parameter mapping [17]. Secondly, starting from a completely general bianisotropic metasurface, this approach naturally reveals the three diffraction-free conditions derived in [14], and ultimately leads to closed-form expressions for the bianisotropic susceptibility tensors. Finally, we provide an experimentally demonstrate two diffraction-free bianisotropic reciprocal refractive metasurfaces.

The paper is organized as follows. Section II presents the GSTC synthesis of the metasurface susceptibility tensors and discusses the physics of the metasurfaces corresponding to the three above options. Next, Sec. III maps the synthesized susceptibilities onto scattering parameters as an intermediate step to discretize the metasurface. Using this mapping, Sec. IV determines the scattering particles corresponding to each metasurface cell. Simulation and experimental validations are provided in Sec. V. Finally, conclusions are given in Sec. VI.

II. REFRACTIVE TRANSVERSE METASURFACE SYNTHESIS

A. Generalized Refraction and GSTC Synthesis

The problem of diffraction-free generalized refraction by a metasurface is represented in Fig. 1. The metasurface is placed at $z = 0$ in the xy -plane of a cartesian coordinate system. We denote a and b the media, possibly having different electromagnetic properties, bounding the metasurface at $z < 0$ and $z > 0$, respectively. A plane wave, with electric and magnetic fields \mathbf{E}_{a1} and \mathbf{H}_{a1} , respectively, impinges from medium a at angle θ_a onto the metasurface. The metasurface transforms, without any spurious reflection and scattering, this wave into a plane wave, with fields \mathbf{E}_{b1} and \mathbf{H}_{b1} , propagating in medium b at angle θ_b .

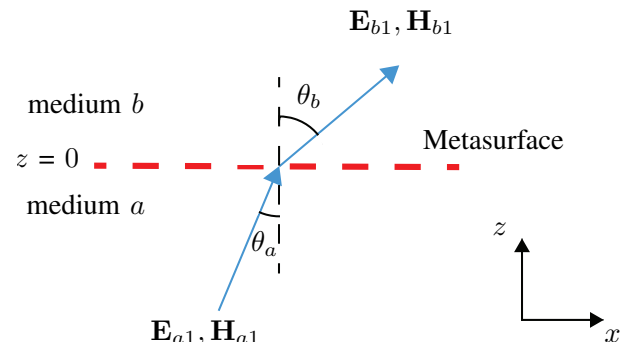


Fig. 1. Problem of diffraction-free generalized refraction by a metasurface.

We shall next perform the synthesis of the diffraction-free generalized refractive metasurface in Fig. 1 using the GSTC-susceptibility technique presented in [17]. This technique consists in specifying the incident, reflected and transmitted fields and computing the corresponding metasurface susceptibility tensors via GSTCs. According to the definition of diffraction-free generalized refraction, the reflected field will be specified to be zero and the transmitted field will be specified as a pure plane wave without any spurious diffraction orders. In the case of a general transverse bianisotropic metasurface, the GSTCs, defined at $z = 0$, are given as

$$\hat{z} \times \Delta \mathbf{H} = j\omega\epsilon_0 \bar{\chi}_{ee} \mathbf{E}_{av} + j\omega \bar{\chi}_{em} \sqrt{\mu_0 \epsilon_0} \mathbf{H}_{av}, \quad (1a)$$

$$\Delta \mathbf{E} \times \hat{z} = j\omega\mu_0 \bar{\chi}_{mm} \mathbf{H}_{av} + j\omega\mu_0 \bar{\chi}_{me} \sqrt{\epsilon_0/\mu_0} \mathbf{E}_{av}, \quad (1b)$$

where the Δ symbol and 'av' subscript represent the differences and averages of the tangential electric or magnetic fields on both sides of the metasurface, and $\bar{\chi}_{ee}$, $\bar{\chi}_{em}$, $\bar{\chi}_{me}$, $\bar{\chi}_{mm}$ are the bianisotropic susceptibility tensors describing the metasurface. In order to realize the simplest and most fundamental generalized refraction operation, we require the metasurface to be non-gyrotropic so as to avoid polarization alteration. As a result, the s-polarization and p-polarization problems are independent from each other and can therefore be treated separately. We shall therefore, without loss of generality, only treat the p-polarization problem.

B. Monoanisotropic Metasurface

We heuristically start with a metasurface having the simplest constitutive parameters, a *monoanisotropic* metasurface. In the p-polarization case, for which the metasurface appears monoisotropic, the fields corresponding to the scenario of Fig. 1 are

$$\mathbf{E}_{a1} = (\cos \theta_a \hat{x} + \sin \theta_a \hat{z}) e^{-j(k_{ax}x + k_{az}z)}, \mathbf{H}_{a1} = \frac{e^{-jk_{ax}x}}{\eta_a} \hat{y}, \quad (2a)$$

$$\mathbf{E}_{b1} = T_p (\cos \theta_b \hat{x} + \sin \theta_b \hat{z}) e^{-j(k_{bx}x + k_{bz}z)}, \mathbf{H}_{b1} = T_p \frac{e^{-jk_{bx}x}}{\eta_b} \hat{y}, \quad (2b)$$

where T_p is the (parallel-polarization) transmission coefficient, $\eta_{(a,b)} = \sqrt{\mu_{(a,b)}/\epsilon_{(a,b)}}$, and

$$k_{(a,b)x} = k_{a,b} \sin \theta_{a,b}, \quad (3a)$$

$$k_{(a,b)z} = k_{a,b} \cos \theta_{a,b}, \quad (3b)$$

where $k_{(a,b)} = \sqrt{\mu_{(a,b)}\epsilon_{(a,b)}}k_0$ with $k_0 = \omega/c_0$.

Based on the above assumption of a transverse metasurface, the GSTCs (1) involve only the x and y components of these fields, evaluated at $z = 0$, which, also accounting for the p-polarization monoisotropy, results into

$$\chi_{ee}^{xx} = \frac{-\Delta H_{y1}}{j\omega\epsilon_0 E_{x,av1}}, \quad (4a)$$

$$\chi_{mm}^{yy} = \frac{-\Delta E_{x1}}{j\omega\mu_0 H_{y,av1}}, \quad (4b)$$

with

$$\Delta E_{x1} = E_{bx1} - E_{ax1} = T_p \cos \theta_b e^{-jk_{bx}x} - \cos \theta_a e^{-jk_{ax}x}, \quad (5a)$$

$$\Delta H_{y1} = H_{by1} - H_{ay1} = T_p e^{-jk_{bx}x}/\eta_b - e^{-jk_{ax}x}/\eta_a, \quad (5b)$$

$$E_{x,av1} = \frac{E_{ax1} + E_{bx1}}{2} = \frac{\cos \theta_a e^{-jk_{ax}x} + T_p \cos \theta_b e^{-jk_{bx}x}}{2} \quad (5c)$$

$$H_{y,av1} = \frac{H_{ay1} + H_{by1}}{2} = \frac{e^{-jk_{ax}x}/\eta_a + T_p e^{-jk_{bx}x}/\eta_b}{2} \quad (5d)$$

where the subscript '1' has been introduced for later convenience. The only unknown in these relations is the transmission coefficient,

T_p . This coefficient may be obtained by enforcing power conservation across the metasurface,

$$\frac{1}{2} \text{Re} ((E_{ax1} \hat{x}) \times (H_{ay1}^* \hat{y})) = \frac{1}{2} \text{Re} ((E_{bx1} \hat{x}) \times (H_{by1}^* \hat{y})), \quad (6)$$

whose resolution for T_p with (2) yields

$$T_p = \sqrt{\frac{\eta_b \cos \theta_a}{\eta_a \cos \theta_b}} \quad (7)$$

which is thus a fundamental *condition for power conserving diffraction-free refraction*.

Inserting (5) into (4) yields the periodic complex susceptibility functions

$$\text{Re}(\chi_{ee}^{xx}) = \frac{-2k_a k_b T_p (\eta_a k_b k_{az} + \eta_b k_a k_{bz}) \sin(\alpha x)}{\epsilon_0 \omega \eta_a \eta_b (k_b^2 k_{az}^2 + k_a^2 k_{bz}^2 T_p^2 + 2k_a k_{az} k_b k_{bz} T_p \cos(\alpha x))}, \quad (8a)$$

$$\text{Im}(\chi_{ee}^{xx}) = \frac{2k_a k_b (\eta_a k_a k_{bz} T_p^2 - \eta_b k_{az} k_b + T_p (\eta_a k_b k_{az} - \eta_b k_a k_{bz}) \cos(\alpha x))}{\epsilon_0 \omega \eta_a \eta_b (k_b^2 k_{az}^2 + k_a^2 k_{bz}^2 T_p^2 + 2k_a k_{az} k_b k_{bz} T_p \cos(\alpha x))}, \quad (8b)$$

$$\text{Re}(\chi_{mm}^{yy}) = \frac{-2\eta_a \eta_b (\eta_a k_{az} k_b + \eta_b k_a k_{bz}) T_p \sin(\alpha x)}{k_a k_b \mu_0 \omega (\eta_b^2 \eta_a^2 T_p^2 + 2\eta_a \eta_b T_p) \cos(\alpha x)}, \quad (8c)$$

$$\text{Im}(\chi_{mm}^{yy}) = \frac{2\eta_a \eta_b (\eta_a k_a k_{bz} T_p^2 - \eta_b k_{az} k_b + (\eta_a k_a k_{bz} T_p^2 - \eta_b k_b k_{az}) T_p^2 \cos(\alpha x))}{k_a k_b \mu_0 \omega (\eta_b^2 \eta_a^2 T_p^2 + 2\eta_a \eta_b T_p) \cos(\alpha x)}, \quad (8d)$$

with $\alpha = k_{ax} - k_{bx}$. Plots of these functions may be found in [8]. The non-zero imaginary parts of χ_{ee}^{xx} and χ_{mm}^{yy} , tensorially corresponding to the loss and gain relations $\bar{\chi}_{ee}^T \neq \bar{\chi}_{ee}^*$ and $\bar{\chi}_{mm}^T \neq \bar{\chi}_{mm}^*$, where the superscripts T and $*$ denote the transpose and conjugate operation respectively [29], indicate the presence of loss (negative imaginary part) and gain (positive imaginary part) alternating along the metasurface. This synthesis corresponds to the first way of obtaining a diffraction-free refractive metasurface, as shown in [14].

C. Bianisotropic Metasurface

Since specifying a monoanisotropic (or monoisotropic) metasurface leads only to the loss and gain option for diffraction-free refraction, as just found, complexity must be added to the metasurface to obtain the nonreciprocity and bianisotropy options. The non-gyrotropy assumption requires $\chi_{ee,mm}^{xy} = \chi_{ee,mm}^{yx} = \chi_{ee,me}^{xx} = \chi_{em,me}^{yy} = 0$, and hence eliminates 8 of the 16 terms of a transverse metasurface, and, among the remaining 8 terms, 4 are for p-polarization and 4 are for s-polarization. Therefore, still assuming p-polarization, only the *bianisotropic* two terms χ_{em}^{xy} and χ_{me}^{yx} can be added to χ_{ee}^{xx} and χ_{mm}^{yy} . This 4-element susceptibility set allows for two fundamentally new possibilities: a) $\chi_{em}^{xy} \neq -\chi_{me}^{yx}$, and b) $\chi_{em}^{xy} = -\chi_{me}^{yx}$. The latter tensorially generalizes to $\bar{\chi}_{em} = -\bar{\chi}_{me}^T$, where the superscript 'T' represents the transpose operation, which is the only condition for *reciprocity* in the prevailing non-gyrotropic situation [29], and the former corresponds thus to a *nonreciprocal* metasurface. These two possibilities correspond to options 2) and 3), respectively, in [14]. In each of the two cases, one has to describe the phenomenon (reciprocity or nonreciprocity) by also specifying the transformation in the reverse direction, namely the direction from medium b to medium a , which brings about two additional equations, leading to a full-rank matrix system of order 4.

In the nonreciprocal case, one may specify any reverse transformation, such as for instance refraction in different directions or

absorption. However, as mentioned in Sec. I, we are primarily interested here in realizing a reciprocal metasurface. The corresponding reverse transformation, involving the same angles as in Fig. 1, is shown in Fig. 2. Thus, the proper synthesis equations, including

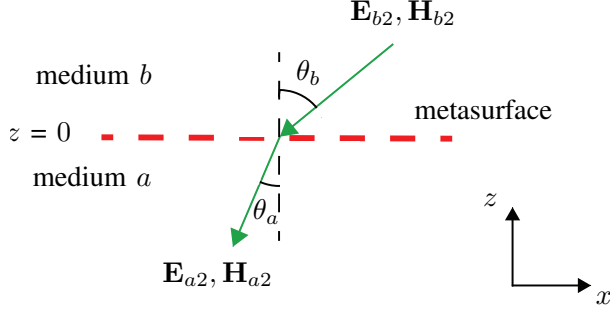


Fig. 2. Reverse transformation reciprocal to that of Fig. 1.

both the reciprocal direct (subscript ‘1’) and reverse (subscript ‘2’) transformations, may be compactly written as

$$\begin{bmatrix} \Delta H_{y1} & \Delta H_{y2} \\ \Delta E_{x1} & \Delta E_{x2} \end{bmatrix} = \begin{bmatrix} -j\omega\epsilon_0\chi_{ee}^{xx} & -jk_0\chi_{em}^{xy} \\ -jk_0\chi_{me}^{yx} & -j\omega\mu_0\chi_{mm}^{yy} \end{bmatrix} \begin{bmatrix} E_{x1,av} & E_{x2,av} \\ H_{y1,av} & H_{y2,av} \end{bmatrix}, \quad (9)$$

whose first and second columns correspond to the direct and reverse transformations, respectively. The fields corresponding to the reverse transformation [Fig. 2] read

$$\mathbf{E}_{a2} = -(\cos\theta_a\hat{x} + \sin\theta_a\hat{z})e^{j(k_{ax}x + k_{az}z)}, \quad \mathbf{H}_{a2} = \frac{e^{jk_{ax}x}}{\eta_a}\hat{y}, \quad (10a)$$

$$\mathbf{E}_{b2} = -T_p(\cos\theta_b\hat{x} + \sin\theta_b\hat{z})e^{j(k_{bx}x + k_{bz}z)}, \quad \mathbf{H}_{b2} = T_p\frac{e^{jk_{bx}x}}{\eta_b}\hat{y}, \quad (10b)$$

corresponding to

$$\Delta E_{x2} = E_{bx2} - E_{ax2} = -T_p\cos\theta_b e^{jk_{bx}x} + \cos\theta_a e^{jk_{ax}x}, \quad (11a)$$

$$\Delta H_{y2} = H_{by2} - H_{ay2} = T_p e^{jk_{bx}x}/\eta_b - e^{jk_{ax}x}/\eta_a, \quad (11b)$$

$$E_{x,av2} = \frac{E_{ax2} + E_{bx2}}{2} = \frac{-\cos\theta_a e^{jk_{ax}x} - T_p\cos\theta_b e^{jk_{bx}x}}{2}, \quad (11c)$$

$$H_{y,av2} = \frac{H_{ay2} + H_{by2}}{2} = \frac{e^{jk_{ax}x}/\eta_a + T_p e^{jk_{bx}x}/\eta_b}{2}. \quad (11d)$$

Inserting (5) and (11) into (9) finally yields the sought after transverse susceptibility functions

$$\chi_{ee}^{xx} = \frac{-4k_a k_b T_p \sin(\alpha x)}{\epsilon_0\omega (T_p(\eta_a k_b k_{az} + \eta_b k_a k_{bz}) \cos(\alpha x)) + \eta_a k_b k_{az} + \eta_b k_a k_{bz} T_p^2}, \quad (12a)$$

$$\chi_{em}^{xy} = \frac{2j (T_p(\eta_a k_b k_{az} - \eta_b k_a k_{bz}) \cos(\alpha x)) - \eta_b k_b k_{az} + \eta_a k_a k_{bz} T_p^2}{k_0 (T_p(\eta_a k_b k_{az} + \eta_b k_a k_{bz}) \cos(\alpha x)) + \eta_a k_b k_{az} + \eta_b k_a k_{bz} T_p^2}, \quad (12b)$$

$$\chi_{me}^{yx} = \frac{2j (T_p(\eta_b k_b k_{az} - \eta_a k_b k_{az}) \cos(\alpha x)) - \eta_b k_b k_{az} + \eta_a k_a k_{bz} T_p^2}{k_0 (T_p(\eta_a k_b k_{az} + \eta_b k_a k_{bz}) \cos(\alpha x)) + \eta_a k_b k_{az} + \eta_b k_a k_{bz} T_p^2}, \quad (12c)$$

$$\chi_{mm}^{yy} = \frac{-4\eta_a \eta_b k_{az} k_{bz} T_p \sin(\alpha x)}{\mu_0\omega (T_p(\eta_a k_b k_{az} + \eta_b k_a k_{bz}) \cos(\alpha x)) + \eta_a k_b k_{az} + \eta_b k_a k_{bz} T_p^2}, \quad (12d)$$

with $\alpha = k_{ax} - k_{bx}$. These relations are plotted in Fig. 3 for $\theta_a = 0^\circ$ and $\theta_b = 70^\circ$, and considering air on both sides of the metasurface.

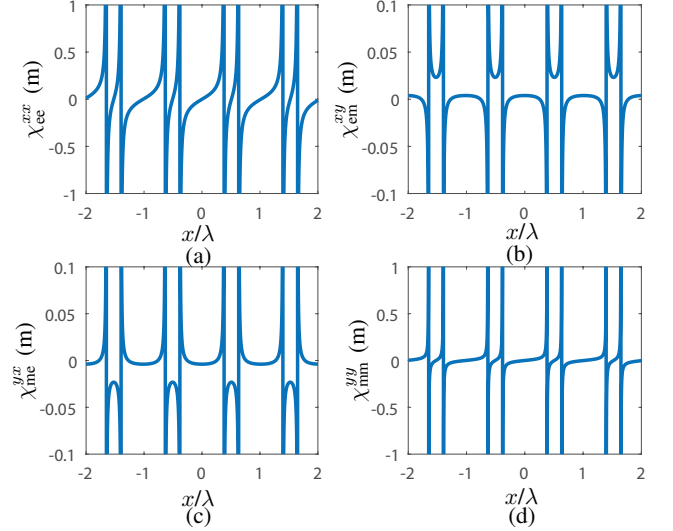


Fig. 3. Susceptibility functions (12) for $\theta_a = 0^\circ$ and $\theta_b = 70^\circ$. (a) χ_{ee}^{xx} (purely real). (b) χ_{em}^{xy} (purely imaginary). (c) χ_{me}^{yx} (purely imaginary). (d) χ_{mm}^{yy} (purely real).

D. Properties of the Synthesized Metasurface

The metasurface characterized by the susceptibilities in (12) possesses the following properties:

- It is *bianisotropic*, as already noted in Sec. II-C, since $\chi_{em}^{xy} \neq 0$ and $\chi_{me}^{yx} \neq 0$.
- As a result of bianisotropy, it is *asymmetric*, as will be shown in the corresponding scattering parameters to be given in Sec. III.
- It is *reciprocal*, as noted in Sec. II-C, since $\chi_{em}^{xy} = -\chi_{me}^{yx}$, which is equivalent to $T_p = \sqrt{\eta_b \cos\theta_a / \eta_a \cos\theta_b}$ (power conservation), tensorially corresponding to the relation $\overline{\chi}_{me}^T = -\overline{\chi}_{em}^*$.
- It is *passive* and *lossless*, since $\chi_{ee}^{xx}, \chi_{mm}^{yy} \in \mathbb{R}$ and $\chi_{em}^{xy}, \chi_{me}^{yx} \in \mathbb{I}$, tensorially corresponding to the relations $\overline{\chi}_{ee}^T = \overline{\chi}_{ee}^*$, $\overline{\chi}_{mm}^T = \overline{\chi}_{mm}^*$ and $\overline{\chi}_{me}^T = \overline{\chi}_{em}^*$ [29].
- It is *periodic* in x with period $k_{ax} - k_{bx}$, as seen in Fig. 3, corresponding to the periodic field momentum transformation [30] operated by the metasurface.
- Since it is periodic, it inherently supports an *infinite number of space harmonics* [31]. From the fact that the metasurface is synthesized so as to scatter only in one direction, all the space harmonics (or diffraction orders) *other than that corresponding to the specified refraction angle* must be *evanescent* (i.e. transformed to leaky or surface waves).

III. SCATTERING PARAMETER MAPPING

The task now is to establish a proper link between the mathematical transverse susceptibility functions (12) and the corresponding real metasurface, composed of an array of scattering particles. Specifically, this includes discretizing these susceptibility functions in sub-wavelength cells and determining the appropriate particle geometries for all the cells.

To build a metasurface with the assumed purely transverse susceptibility, $\overline{\chi}_i$, we shall proceed as follows:

- 1) Map the synthesized susceptibility parameters onto *normal-incidence* scattering parameters. The reason to use normal incidence *in the design procedure* is twofold. First, this is a necessary condition to ensure that only the *transverse* terms of the particle susceptibilities or, more precisely, polarizabilities, get excited². Second, this will lead to the *simplest* possible simulation set-up for each specific particle (step 3 below), obliqueness being produced by the phase gradient between cells. For p-polarization, and assuming that the metasurface is reciprocal and surrounded by air, the corresponding relations are found, following the procedure in [17], as

$$S_{11}^{xx} = \frac{-2j(2k_0\eta_0\chi_{me}^{yx} + \mu_0\omega\chi_{mm}^{yy} - \eta_0^2\epsilon_0\omega\chi_{ee}^{xx})}{D^{xx}}, \quad (13a)$$

$$S_{22}^{xx} = \frac{2j(2k_0\eta_0\chi_{me}^{yx} - \mu_0\omega\chi_{mm}^{yy} + \eta_0^2\epsilon_0\omega\chi_{ee}^{xx})}{D^{xx}}, \quad (13b)$$

$$S_{21}^{xx} = S_{12}^{xx} = \frac{-j\eta_0(4 + k_0^2(\chi_{me}^{yx})^2 + \mu_0\epsilon_0\omega^2\chi_{ee}^{xx}\chi_{mm}^{yy})}{D^{xx}}. \quad (13c)$$

with

$$D^{xx} = -2j\mu_0\omega\chi_{mm}^{yy} + \eta_0(-4 + k_0^2(\chi_{me}^{yx})^2 + \epsilon\omega\chi_{ee}^{xx}(-2j\eta_0 + \mu_0\omega\chi_{mm}^{yy})), \quad (13d)$$

where the x 's in the superscript xx correspond to the transverse component of the p-polarized fields [Eqs. (2) and (10)], assuming also non-gyrotropy. We have thus obtained the scattering matrix periodic functions $\overline{S}^{xx}(x, y)$ corresponding to $\overline{\chi}_{\parallel}(x, y)$. As announced in Sec. II-D, Eqs. (13a) and (13a) reveal that the metasurface is asymmetric, since $S_{11}^{xx} \neq S_{22}^{xx}$.

- 2) Discretize the periodic functions (13), or $\overline{S}^{xx}(x, y)$, in sub-wavelength cells in order to ensure their safe sampling in terms of Nyquist theorem. This leads to the discrete function $\overline{S}^{xx}(x_i, y_j)$, for i, \dots, N_x and j, \dots, N_y , where N_x and N_y represent the number of cells along the x and y directions, respectively.
- 3) Select a generic particle structure and geometry that may be adjusted to cover the phase and amplitude range of $\overline{S}^{xx}(x_i, y_j)$ across the entire metasurface. For simplicity and computational efficiency, compute the scattering parameters (under normal incidence) of each cell separately and within *periodic boundary conditions*. Even though the final metasurface will be locally aperiodic, i.e. made of different adjacent cells, periodic boundary conditions will reasonably approximate the coupling to slightly different neighbours.
- 4) Since $\overline{S}^{xx}(x_i, y_j)$ is periodic, the period includes the complete set of all the different cells, and the overall structure will consist in the periodic repetition of the corresponding *super-cell*. Now, simulate this supercell within periodic boundary conditions with the specified incidence angle, and optimize the geometry of the particles so as to maximize energy refraction in the specified direction, i.e., specifically, in the proper diffraction order corresponding to the supercell.

²In the most general case of full-tensor bianisotropic metasurface, one would have to realize 36 parameters (Footnote 1). Given that GSTCs are composed of 4 (transverse) equations, such a design would in principle demand to specify $36/4 = 9$ transformations across the unit cell, including oblique incidence, which would be prohibitively complicated. Restricting the incidence to be normal, we ensure to select out and realize only the 16 transverse susceptibilities, which corresponds to $16/4 = 4$ transformations, 2 for each polarization (p and s) and, for each polarization, 2 for each incidence side (Fig. 1 and Fig. 2). This eventually requires only a simple normal-incidence scattering simulation for each z -direction.

Note that it is practically difficult to realize scattering particles with purely transverse polarizability and hence purely transverse susceptibility. Practical metasurfaces typically always include small non-zero longitudinal susceptibility terms, $\overline{\chi}_{\perp}(x, y)$. Such terms are not excited in 3) above, due to normal incidence, but would play a role in 4) above, given the oblique angle³. We shall select a generic particle without longitudinal metallizations, to avoid strong perpendicular electric moments, and without transverse loops, to avoid strong perpendicular magnetic moments. We may therefore expect negligible $\overline{\chi}_{\perp}(x, y)$ and a design essentially correspond to the assumed purely transverse one.

IV. DESIGN OF SCATTERING PARTICLES

We shall design here two diffraction-free refractive transverse metasurfaces to illustrate the theory of the previous sections: the first metasurface with $(\theta_a, \theta_b) = (20^\circ, -28^\circ)$ at 10 GHz and the second with $(\theta_a, \theta_b) = (0^\circ, -70^\circ)$ at 10.5 GHz. For this purpose, we shall follow the procedure described in Sec. III. For experimental simplicity, we assume that the metasurface is entirely surrounded by free space ($k_a = k_b = k_0$, $\eta_a = \eta_b = \eta_0$).

As the step 1), we insert the susceptibilities given by (12), with $k_a = k_b = k_0$, into (13). This yields the scattering parameter functions

$$S_{11}^{xx} = \frac{(-k_0^2 + k_{az}k_{bz}) \sin[(k_{ax} - k_{bx})x] + jk_0(k_{az} - k_{bz}) \cos[(k_{ax} - k_{bx})x]}{(k_0^2 + k_{az}k_{bz}) \sin[(k_{ax} - k_{bx})x] + jk_0(k_{az} + k_{bz}) \cos[(k_{ax} - k_{bx})x]}, \quad (14a)$$

$$S_{22}^{xx} = \frac{(-k_0^2 + k_{az}k_{bz}) \sin[(k_{ax} - k_{bx})x] - jk_0(k_{az} - k_{bz}) \cos[(k_{ax} - k_{bx})x]}{(k_0^2 + k_{az}k_{bz}) \sin[(k_{ax} - k_{bx})x] + jk_0(k_{az} + k_{bz}) \cos[(k_{ax} - k_{bx})x]}, \quad (14b)$$

$$S_{12}^{xx} = S_{21}^{xx} = \frac{2jk_0\sqrt{k_{az}k_{bz}}}{(k_0^2 + k_{az}k_{bz}) \sin[(k_{ax} - k_{bx})x] + jk_0(k_{az} + k_{bz}) \cos[(k_{ax} - k_{bx})x]}. \quad (14c)$$

It may a priori seem contradictory with the initial assumption of reflection-less refraction to obtain $S_{11}^{xx} \neq 0$ and $S_{22}^{xx} \neq 0$. However, there is no contradiction if one recalls that Eqs. (13) are associated in the *design procedure* with *normal incidence*, both to isolate out transverse susceptibility components and to simulate the cells one by one, whereas the specified incidence angle is generally nonzero. When excited under the specified oblique incidence angle, the metasurface realized by this design methodology will naturally be reflection-less. Note that the metasurface asymmetry predicted in Sec II-D is still clearly apparent from the fact that $S_{11}^{xx} \neq S_{22}^{xx}$, since asymmetry for normal incidence implies asymmetry.

As step 2), we discretize each of the two metasurfaces in 6 different unit cells of size 6×6 mm ($\sim \lambda_0/5$) for the metasurface with $(\theta_a, \theta_b) = (20^\circ, -28^\circ)$ and 5.1×5.1 mm ($\sim \lambda_0/5.6$) for the metasurface with $(\theta_a, \theta_b) = (0^\circ, -70^\circ)$.

As step 3), we choose scattering particles made of three dog-bone shaped metallic layers separated by 1.52 mm-thick ($\sim \lambda_0/20 = \lambda_d/11.55$) Rogers 3003 ($\epsilon_r = 3$, $\tan \delta = 0.0013$) dielectric slabs. The generic dog-bone metallization is shown in Fig. 4 (a), while Fig. 4 (b) shows the corresponding three-layer unit cell. Each unit

³The final design may thus, rigorously, include a small $\overline{\chi}_{\perp}(x, y)$ associated with a slightly modified $\overline{\chi}_{\parallel}(x, y)$. Such a metasurface would strictly correspond to a diffraction-free-refraction design different than the initially purely transverse one. This does not represent any contradiction since the synthesis corresponds to an *inverse problem*, naturally admitting multiple solutions.

TABLE I
DIMENSIONS OF THE UNIT CELLS FOR THE $(\theta_a, \theta_b) = (20^\circ, -28^\circ)$
METASURFACE.

		W	L	G	S
Cell 1	Layer 1	4.25	0.5	0.75	0.5
	Layer 2	3.125	0.5	0.5	0.875
	Layer 3	2.5	0.5	0.25	0.5
Cell 2	Layer 1	3.25	0.5	0.5	0.5
	Layer 2	1.75	0.5	0.5	0.25
	Layer 3	3.25	0.5	0.5	0.5
Cell 3	Layer 1	3.625	0.5	1	0.5
	Layer 2	3	0.5	0.75	0.5
	Layer 3	2.625	0.5	0.5	0.5
Cell 4	Layer 1	2.25	0.5	0.5	0.5
	Layer 2	4.75	0.5	0.75	0.5
	Layer 3	4.5	0.5	1	0.5
Cell 5	Layer 1	4.25	0.5	1	0.5
	Layer 2	4.25	0.5	3.75	0.5
	Layer 3	2.375	0.5	0.5	0.5
Cell 6	Layer 1	3	0.5	1.25	0.5
	Layer 2	4.125	0.5	0.5	0.5
	Layer 3	1.5	0.5	1	0.5

TABLE II
DIMENSIONS OF THE UNIT CELLS FOR THE $(\theta_a, \theta_b) = (0^\circ, -70^\circ)$
METASURFACE.

		W	L	G	S
Cell 1	Layer 1	3	0.5	0.375	0.5
	Layer 2	2.5	0.5	0.375	0.5
	Layer 3	4	0.5	0.25	0.5
Cell 2	Layer 1	3.25	0.5	0.25	0.5
	Layer 2	3	0.5	0.5	0.5
	Layer 3	2.5	0.5	0.25	0.5
Cell 3	Layer 1	4	0.5	0.75	0.5
	Layer 2	3.75	0.5	0.75	0.5
	Layer 3	2.5	0.5	0.5	0.5
Cell 4	Layer 1	3.25	0.5	0.625	0.5
	Layer 2	1.5	0.5	1	0.5
	Layer 3	2	0.5	0.875	0.5
Cell 5	Layer 1	4.5	0.5	0.75	0.5
	Layer 2	4.5	0.5	0.625	0.5
	Layer 3	4.25	0.5	1	0.5
Cell 6	Layer 1	3.25	0.5	0.875	0.5
	Layer 2	4.25	0.5	0.5	0.5
	Layer 3	4	0.5	1	0.5

cell is then optimized with periodic conditions using a commercial software (CST Studio 2014), which provides a reasonable initial guess for the geometry of the dog-bone patterns.

As step 4), we combine the six different unit cells into a supercell, which is periodically repeated to form the whole metasurface. Figure 4 (c) and (d) show the generic structure of the supercell. Finally, the supercell, automatically taking into account the exact (as opposed to periodic) coupling between adjacent unit cells, is optimized. Specifically, we simulate the Floquet space harmonics of the supercell and adjust the geometrical parameters so as to maximize the energy in the desired mode. The dimensions (in mm) of the metallic structures of the different unit cells are listed in Tabs. I and II for the two metasurfaces.

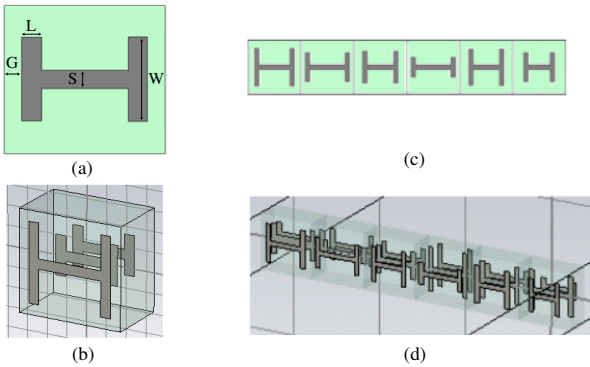


Fig. 4. Metasurface scattering particles. (a) Unit cell front view with dog-bone shaped metallic particle. (b) Unit cell perspective view with dielectric substrates made transparent for visualisation. (c) Supercell composed of 6 unit cells, front view. (d) Supercell perspective view.

V. SIMULATION AND EXPERIMENT

The full-wave simulated fields of the two diffraction-free bianisotropic reciprocal refractive metasurfaces are plotted in Fig. 5. Being perfectly periodic, the metasurface supports in principle an infinite number of space harmonics, as mentioned in the last item of Sec. II-D. In both designs, only the space harmonics $m = 0$, $m = -1$ and $m = +1$ are propagating, while the others are evanescent, and the incident and refracted waves correspond to

the space harmonics $m = 0$ and $m = -1$, respectively. Ideally, from synthesis, 100% of the scattered power should reside in the $m = -1$ space harmonic. Practically, the harmonics R_0 , R_{-1} , R_{+1} , T_0 and T_{+1} are also weakly excited, due to the imperfections of the metasurface associated with discretization and fabrication restrictions (essentially limited resolution of the metallic particles), already taken into account at this simulation stage.

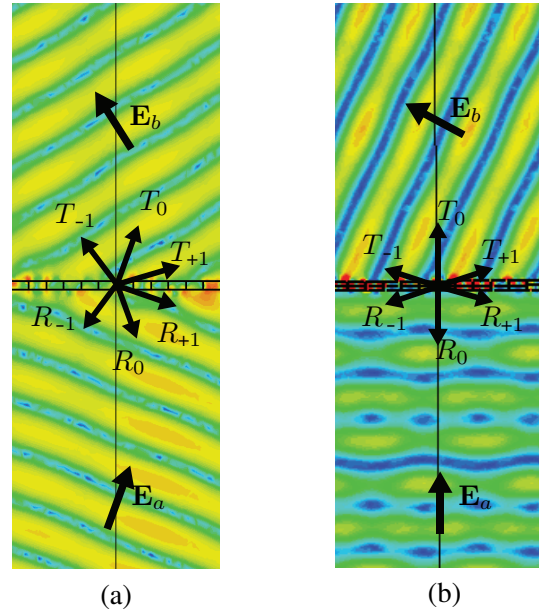


Fig. 5. Full-wave simulated electric field magnitude for the two diffraction-free bianisotropic reciprocal refractive metasurfaces. The horizontal extent of each figure corresponds to two supercells. The propagating field includes the reflected (R) and transmitted (T) space harmonics $m = 0$, $m = -1$ and $m = +1$, whose directions are indicated by the arrows in the center, while the other space harmonics are evanescent. (a) Metasurface with $(\theta_a, \theta_b) = (20^\circ, -28^\circ)$ at 10 GHz. (b) Metasurface with $(\theta_a, \theta_b) = (0^\circ, -70^\circ)$ at 10.5 GHz.

The corresponding scattering parameter simulations are shown in Fig. 6 and Fig. 7 for the $(\theta_a, \theta_b) = (20^\circ, -28^\circ)$ metasurface and the $(\theta_a, \theta_b) = (0^\circ, -70^\circ)$ metasurface, respectively. As expected from

synthesis, most of the incident power, except for small conducting and dielectric dissipation loss and negligible coupling to undesired space harmonics, is refracted to the specified direction (~ -0.6 dB for the $(\theta_a, \theta_b) = (20^\circ, -28^\circ)$ metasurface and ~ -0.9 dB for the $(\theta_a, \theta_b) = (0^\circ, -70^\circ)$ metasurface) with low reflection (< -15 dB).

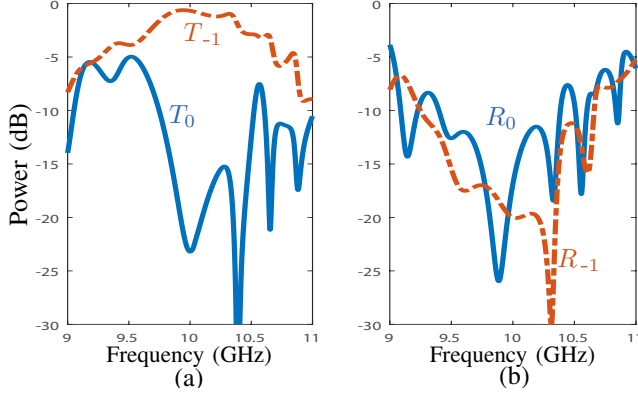


Fig. 6. Scattering parameters of the $(\theta_a, \theta_b) = (20^\circ, -28^\circ)$ 10 GHz metasurface. (a) Transmitted propagating space harmonics. (b) Reflected propagating space harmonics. The T_{+1} and R_{+1} harmonics are also propagating but not visible in these graphs as their magnitudes are lower than -80 dB.

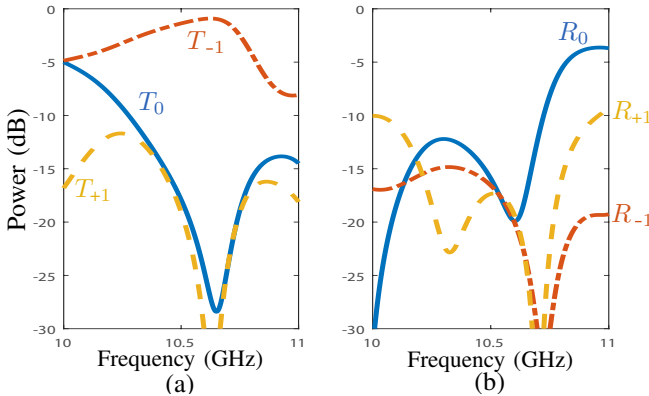


Fig. 7. Scattering parameters of the $(\theta_a, \theta_b) = (0^\circ, -70^\circ)$ 10.5 GHz metasurface. (a) Transmitted propagating space harmonics. (b) Reflected propagating space harmonics. (Note that the optimum has been up-shifted by around 0.1 GHz in the optimization procedure.)

The two metasurfaces were fabricated and measured. Figure 8 shows a photograph of them. In the measurement, we used a horn antenna placed ~ 400 mm from the metasurface and a near-field probe scanning over a plane parallel to the metasurface in the transmission region. We then applied a near-field to far-field transformation [32] to evaluate the transmission response of the metasurface. The measurement results are shown, superimposed with the simulations, in Figs. 9 and 10 for the $(\theta_a, \theta_b) = (20^\circ, -28^\circ)$ metasurface and the $(\theta_a, \theta_b) = (0^\circ, -70^\circ)$ metasurface, respectively. The observed discrepancies between simulation and measurement may be attributed to different factors, including fabrication tolerance, horn antenna excitation (instead of ideal plane wave) and probe antenna imperfection (spurious edge diffraction).

The performance of our metasurfaces is limited only by dissipation loss in the metal scatterers and in the dielectric. In [33], the authors established a theoretical limit in efficiency for a lossless

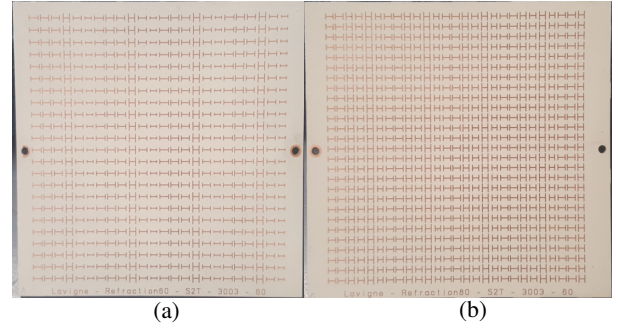


Fig. 8. Photographs of the two fabricated metasurfaces. (a) $(\theta_a, \theta_b) = (20^\circ, -28^\circ)$ metasurface. (b) $(\theta_a, \theta_b) = (0^\circ, -70^\circ)$ metasurface.

monoanisotropic metasurface, which is found to be $\sim 76\%$ for $(\theta_a, \theta_b) = (0^\circ, -70^\circ)$; it is interesting to note that our bianisotropic metasurface exceeds this lossless monoanisotropic limit by around 5% despite the natural presence of loss. The experimental work in [20], for a similar wide-angle refraction, had lower efficiency due to higher scattering into other diffraction orders and higher absorption compared to our metasurface.

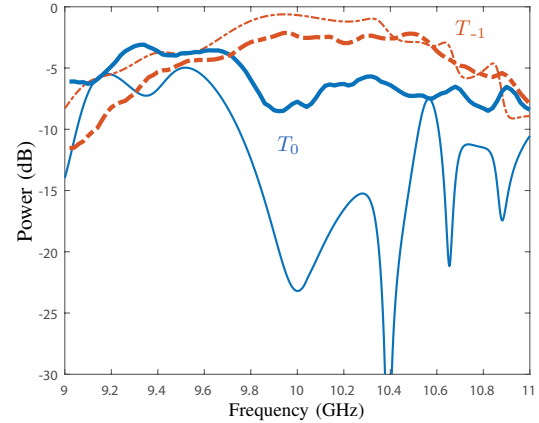


Fig. 9. Measured (thick lines) and simulated (thin lines) scattering parameters in transmission of the $(\theta_a, \theta_b) = (20^\circ, -28^\circ)$ metasurface.

VI. CONCLUSION

We have derived the conditions for diffraction-free refraction in a metasurface using a medium-based approach based on Generalized Sheet Transition Conditions (GSTCs) and surface susceptibility tensors, and experimentally demonstrated two diffraction-free metasurfaces that are essentially lossless, passive, bianisotropic and reciprocal.

Following [14], we have considered refractive metasurfaces possessing only *transverse* susceptibility components. However, diffraction-less refraction might also be achieved by metasurfaces including *normal* polarizabilities, which would lead to other possibilities than the three reported in [14]. However, solving the synthesis problem for metasurfaces with nonzero normal susceptibility components is not trivial since the corresponding GSTCs relations form a set of *differential* equations instead of just algebraic equations. At this stage, the design of such structures remains an open avenue for further investigation.

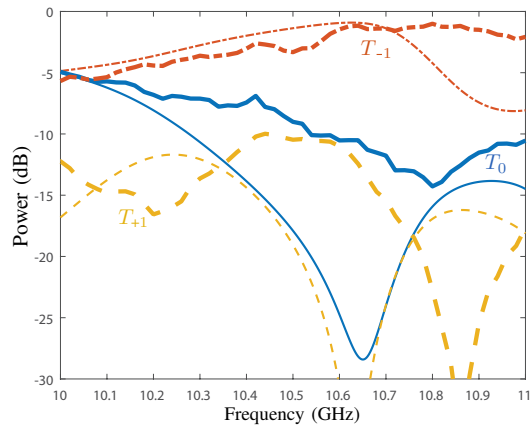


Fig. 10. Measured (thick lines) and simulated (thin lines) scattering parameters in transmission of the $(\theta_a, \theta_b) = (0^\circ, -70^\circ)$ metasurface. Note that the optimal frequency after fabrication was up-shifted by about 0.2 GHz compared to the simulation.

REFERENCES

- [1] S. B. Glybovski, S. A. Tretyakov, P. A. Belov, Y. S. Kivshar, and C. R. Simovski, "Metasurfaces: From microwaves to visible," *Phys. Rep.*, vol. 634, 2016.
- [2] A. M. Urbas, Z. Jacob, L. Dal Negro, N. Engheta, A. Boardman, P. Egan, A. B. Khanikaev, V. Menon, M. Ferrera, N. Kinsey *et al.*, "Roadmap on optical metamaterials," *J. Opt.*, vol. 18, no. 9, p. 093005, 2016.
- [3] S. Tretyakov, "Metasurfaces for general transformations of electromagnetic fields," *Phil. Trans. R. Soc. A*, vol. 373, no. 2049, p. 20140362, 2015.
- [4] Y. Ra'di, V. S. Asadchy, and S. A. Tretyakov, "Total absorption of electromagnetic waves in ultimately thin layers," *IEEE Antenn. Wireless Propag. Lett.*, vol. 61, no. 9, pp. 4606–4614, 2013.
- [5] H. Shi, A. Zhang, S. Zheng, J. Li, and Y. Jiang, "Dual-band polarization angle independent 90 polarization rotator using twisted electric-field-coupled resonators," *Appl. Phys. Lett.*, vol. 104, no. 3, p. 034102, 2014.
- [6] T. S. Almomneef and O. M. Ramahi, "Metamaterial electromagnetic energy harvester with near unity efficiency," *Appl. Phys. Lett.*, vol. 106, no. 15, p. 153902, 2015.
- [7] C. Pfeiffer and A. Grbic, "Controlling vector Bessel beams with metasurfaces," *Phys. Rev. Applied*, vol. 2, no. 4, p. 044012, 2014.
- [8] K. Achouri, G. Lavigne, and C. Caloz, "Comparison of two synthesis methods for birefringent metasurfaces," *J. Appl. Phys.*, vol. 120, no. 23, p. 235305, 2016.
- [9] K. Achouri, G. Lavigne, M. A. Salem, and C. Caloz, "Metasurface spatial processor for electromagnetic remote control," *IEEE Antenn. Wireless Propag. Lett.*, vol. 64, no. 5, pp. 1759–1767, 2016.
- [10] M. Khorasaninejad, W. T. Chen, R. C. Devlin, J. Oh, A. Y. Zhu, and F. Capasso, "Metalenses at visible wavelengths: Diffraction-limited focusing and subwavelength resolution imaging," *Science*, vol. 352, no. 6290, pp. 1190–1194, 2016.
- [11] N. Yu, P. Genevet, M. A. Kats, F. Aieta, J.-P. Tetienne, F. Capasso, and Z. Gaburro, "Light propagation with phase discontinuities: generalized laws of reflection and refraction," *Science*, vol. 334, no. 6054, pp. 333–337, 2011.
- [12] M. Neviere, "Electromagnetic study of transmission gratings," *Appl. Opt.*, vol. 30, no. 31, pp. 4540–4547, 1991.
- [13] N. Destouches, A. Tishchenko, J. Pommier, S. Reynaud, O. Parriaux, S. Tonchev, and M. A. Ahmed, "99% efficiency measured in the 1st order of a resonant grating," *Opt. Express*, vol. 13, no. 9, pp. 3230–3235, 2005.
- [14] V. S. Asadchy, M. Albooyeh, S. N. Tsvetkova, A. Díaz-Rubio, Y. Ra'di, and S. A. Tretyakov, "Perfect control of reflection and refraction using spatially dispersive metasurfaces," *Phys. Rev. B*, vol. 94, p. 075142, Aug 2016.
- [15] N. M. Estakhri and A. Alù, "Wave-front transformation with gradient metasurfaces," *Phys. Rev. X*, vol. 6, no. 4, p. 041008, 2016.
- [16] A. Epstein and G. V. Eleftheriades, "Arbitrary power-conserving field transformations with passive lossless omega-type bianisotropic metasurfaces," *IEEE Trans. Antennas Propag.*, vol. 64, pp. 3880 – 3895, 2016.
- [17] K. Achouri, M. A. Salem, and C. Caloz, "General metasurface synthesis based on susceptibility tensors," *IEEE Trans. Antennas Propag.*, vol. 63, no. 7, pp. 2977–2991, July 2015.
- [18] B. O. Zhu and Y. Feng, "Passive metasurface for reflectionless and arbitrary control of electromagnetic wave transmission," *IEEE Trans. Antennas Propag.*, vol. 63, no. 12, pp. 5500–5511, 2015.
- [19] J. P. Wong, A. Epstein, and G. V. Eleftheriades, "Reflectionless wide-angle refracting metasurfaces," *IEEE Antenn. Wireless Propag. Lett.*, vol. 15, pp. 1293–1296, 2016.
- [20] M. Chen, E. Abdo-Sánchez, A. Epstein, and G. V. Eleftheriades, "Experimental verification of reflectionless wide-angle refraction via a bianisotropic Huygens' metasurface," *arXiv preprint arXiv:1703.06669*, 2017.
- [21] G. Lavigne, K. Achouri, C. Caloz, V. Asadchy, and S. Tretyakov, "Perfectly refractive metasurface using bianisotropy," *arXiv preprint arXiv:1704.01641*, 2017.
- [22] B. Lax and K. J. Button, "Microwave ferrites and ferrimagnetics," 1962.
- [23] T. Kodera, D. L. Sounas, and C. Caloz, "Artificial Faraday rotation using a ring metamaterial structure without static magnetic field," *Appl. Phys. Lett.*, vol. 99, no. 3, p. 031114, 2011.
- [24] Z. Wang, Z. Wang, J. Wang, B. Zhang, J. Huangfu, J. D. Joannopoulos, M. Soljačić, and L. Ran, "Gyrotropic response in the absence of a bias field," *Proc. Natl. Acad. Sci. U.S.A.*, vol. 109, no. 33, pp. 13 194–13 197, 2012.
- [25] S. Taravati, B. A. Khan, S. Gupta, K. Achouri, and C. Caloz, "Nonreciprocal nongyrotropic magnetless metasurface," *IEEE Trans. Antennas Propag.*, 2017.
- [26] K. Achouri, B. A. Khan, S. Gupta, G. Lavigne, M. A. Salem, and C. Caloz, "Synthesis of electromagnetic metasurfaces: principles and illustrations," *EPJ Appl. Metamater.*, vol. 2, p. 12, 2015.
- [27] K. Achouri, Y. Vahabzadeh, and C. Caloz, "Mathematical synthesis and analysis of nonlinear metasurfaces," *arXiv preprint arXiv:1703.09082*, 2017.
- [28] M. M. Idemen, *Discontinuities in the electromagnetic field*. John Wiley & Sons, 2011, vol. 40.
- [29] E. J. Rothwell and M. J. Cloud, *Electromagnetics*. CRC press, 2008.
- [30] M. A. Salem and C. Caloz, "Manipulating light at distance by a metasurface using momentum transformation," *Opt. Express*, vol. 22, no. 12, pp. 14 530–14 543, 2014.
- [31] A. Ishimaru, *Electromagnetic wave propagation, radiation, and scattering*. Prentice-Hall, 1991.
- [32] C. A. Balanis, *Antenna theory: analysis and design*. John Wiley & Sons, 2016.
- [33] M. Selvanayagam and G. V. Eleftheriades, "Discontinuous electromagnetic fields using orthogonal electric and magnetic currents for wavefront manipulation," *Opt. Express*, vol. 21, no. 12, pp. 14 409–14 429, 2013.